Paramagnetic effect at low and high magnetic fields in melt-textured $YBa_2Cu_3O_{7-\delta}$

Fábio Teixeira Dias
Instituto de Física, Universidade Federal do Rio Grande do Sul, P.O. Box 15051, 91501-970 Porto Alegre, Brazil

Paulo Pureur
Instituto de Física, Universidade Federal do Rio Grande do Sul, P.O. Box 15051, 91501-970 Porto Alegre, Brazil

Pedro Rodrigues, Jr.
Departamento de Física, Universidade Estadual de Ponta Grossa, 84031-510 Ponta Grossa, Brazil

Xavier Obradors
Institut de Ciència de Materials de Barcelona, Conseil Superior d'Investigacions Cientifiques, Campus de la Universitat Autònoma de Barcelona, 08193 Bellaterra, Catalunya, Spain

(Received 22 August 2003; revised manuscript received 26 March 2004; published 21 December 2004)

We report on systematic field-cooled magnetization experiments in five different melt-textured $YBa_2Cu_3O_7$ samples containing large amounts of Y_2BaCuO_5 precipitates. These composites were grown with the Bridgman or top-seeding techniques. Fields ranging from 1 Oe up to 50 kOe were applied either parallel or perpendicular to the $Cu\text{-}O_2$ atomic planes. In the low field limit, we observed the paramagnetic Meissner effect (PME) in a Bridgman grown sample for the configuration where the field is oriented parallel to the $Cu\text{-}O_2$ atomic planes. Contrasting with this unique observation at low fields, a paramagnetic response related to the superconducting state was observed in all of the studied samples when strong enough fields were applied in both orientations. This high-field paramagnetic effect shows some noticeable differences when compared to the most frequently reported PME at very low fields. In particular, the magnitude of the high-field paramagnetic moment increases when the field is augmented. Moreover, this effect shows a strong and anomalous relaxation, such that the paramagnetic moment increases as a function of the time. The anisotropy of the high-field paramagnetic moment depends on the sample microstructure, suggesting that pinning by the Y_2BaCuO_5 particles plays a crucial role in the explanation of this effect in the melt-processed $YBa_2Cu_3O_7$ materials.

DOI: 10.1103/PhysRevB.70.224519 PACS number(s): 74.72.Bk, 74.25.Ha, 74.81.Bd

I. INTRODUCTION

The paramagnetic Meissner effect (PME) was first reported in some polycrystalline samples of $Bi_2Sr_2CaCu_2O_x$ (Bi-2212) high temperature superconductors.[1–3] This phenomenon is attributed to the occurrence of a net paramagnetic moment when these materials are cooled through T_c in the presence of low magnetic fields. The discovery of the PME has prompted an enormous effort of investigation due to the striking contrast of this effect with the otherwise expected diamagnetic response. Further motivation was given by its earlier interpretation, based on the occurrence of Josephson π junctions between superconducting grains in the sample.[4] According to this interpretation, the samples showing PME may be modeled as a Josephson medium where the π junctions are randomly distributed. Assuming that closed superconducting loops containing an odd number of these anomalous junctions are likely to occur in these networks, spontaneous and polarizable orbitals currents may be generated, giving origin to the observed PME at very low applied fields. The required π-phase shifts in the Josephson links were proposed to arise from *d*-wave pairing symmetry in the high-T_c suprates.[5]

The concept of polarized orbital currents to explain the low field PME in the Bi-based granular superconductors was further developed by studies of the characteristic microstructure of samples showing this effect,[6] and by investigations on the time dependence of the paramagnetic moment,[7] magnetic imaging using a scanning SQUID microscope,[8] ac susceptibility,[9] magnetic aging,[10] and microwave absorption.[2,3]

Further discoveries about PME, however, challenge the above outlined interpretation. Of paramount importance was the observation of low field PME in Nb samples having the form of mm-sized disks,[11,12] and thin films.[13,14] Although being qualitatively similar to the phenomenon reported in the Bi-based high-T_c cuprates, the effect in Nb was demonstrated to be strongly influenced by the sample geometry and surface. Particularly, polishing the sample surfaces affect the PME significantly, and may lead to its disappearance.[11,12] A surface dependent PME in $YBa_2Cu_3O_{7-\delta}$ (YBCO) single crystals was also found.[15] These results motivated the proposal of mechanisms to explain the PME without taking into account effects from intrinsically nonconventional superconductivity. Thus, models based on flux trapping and flux compression effects were proposed. Nonequilibrium compressed flux states may be stabilized by inhomogeneously cooling the sample, so that its surface becomes superconducting prior to the bulk.[16] Then, the magnetic flux may be pushed into the sample, creating a compressed state upon further cooling. Similarly, the formation of a giant vortex on the sample surface,[17] or the flux capture by samples with a special shape[18] may also produce compression of the trapped flux.

 ©2004 The American Physical Society

The giant vortex mechanism was shown to be responsible for PME in μm-size disks of Al, where transitions between metastable giant vortex states having different angular momenta have been detected.[19] These transitions compress the giant vortex into smaller volumes, allowing extra flux to penetrate in the sample surface and produce a net paramagnetic moment. Recently, the PME was observed in Josephson-junction arrays fabricated from Nb and Al_2O_3.[20,21] Since these systems are relatively simple and may be prepared under well controlled circumstances, the occurrence of PME in this case may help to understand its underlying cause. Indeed, a model for screening in multiply-connected superconductors was proposed to account for the paramagnetism without invoking the role of π junctions.[21] According to this model, the screening of the array is provided by the loops at its boundaries. Thus, diamagnetic currents running at the external perimeter induce currents in the opposite sense in the interior of the array. These inner currents generate an overall paramagnetic offset under certain conditions. Originally, the model adopted the behavior of an effective single loop containing four Josephson junctions as representative of the whole array.[21] However, simulations taking into account the mutual-inductance interactions between loops in the array[22] generalize results obtained in Ref. 21. These calculations confirm that PME might be the dominant response, depending on the field strength and parameters as the self-inductance and capacitance of the Josephson junctions.

Considering that granularity in superconductors emulates a disordered network of Josephson junctions, the PME observed in low-T_c and high-T_c granular superconductors has also been described as an intrinsic effect of multiply-connected superconductors.[14] The interpretation of the PME observed in granular thin films of Nb and YBCO make use of this assumption.

Another important result concerning the paramagnetic response in the superconducting state was obtained by Rykov *et al.*[23] after cooling large YBCO single crystals in strong applied fields. Authors in Ref. 23 called this phenomenon the high-field paramagnetic effect (HFPME) so that it may be distinguished from the low-field PME which is possibly related to the Meissner state. The HFPME was found to depend on the cooling rate and sample size, which suggests that the paramagnetic moment in this case might be induced by flux compression. A recent review of the paramagnetic Meissner effect and related dynamical phenomena, with an emphasis on the theoretical description of the π junctions scenario, is presented in Ref. 24.

In this article, we report on dc magnetization measurements in five different melt-textured samples of YBCO with enhanced pinning characteristics. Experiments were performed in fields ranging from 1 Oe up to 50 kOe applied either parallel or perpendicular to the $Cu\text{-}O_2$ atomic planes (*ab plane*). In low fields ($\mu_0 H < 20$ Oe), paramagnetic moments were detected in one of the samples when the field was applied parallel to the *ab* plane. However, for fields above 20–30 kOe, HFPME was systematically observed in all of the studied samples, regardless of the field orientation. We have found that this high-field paramagnetic effect is qualitatively distinct from the most commonly reported low-field PME. We also investigate the time dependence of the paramagnetic moments in different temperatures and fields. We discuss the results in light of the existing models. We point out the inadequacies of these theories to explain our experiments and suggest some ingredients that might be considered for interpreting this elusive phenomenon in the case of directionally-solidified YBCO, whose most prominent characteristic is the strong flux-pinning capacity.

This article is organized as follows. In Sec. II we describe the samples, their method of preparation and characterization, and briefly refer to the experimental techniques. In Sec. III results are presented separately according they refer to low-field PME, HFPME, and the time dependence of the HFPME. In Sec. IV results are discussed and in Sec. V conclusions are presented. Some preliminary results concerning one of our melt-processed samples were presented in Refs. 25 and 26.

II. EXPERIMENTAL

A. Samples

Five different melt-textured YBCO samples prepared at the Institut de Ciencia de Materiales of Barcelona, Spain, were studied in this work. One of the samples, labeled B1, was cut out from a pellet grown with a Bridgman technique.[27] In this case, the textured YBCO was obtained by directionally re-solidifying a preformed ceramic bar of a composite containing a certain amount of the Y_2BaCuO_5 (Y211) phase. The bar was displaced vertically inside a furnace and heated up to a maximum temperature of 1050 °C. While displacing, the bar was submitted to a longitudinal temperature gradient of 20 °C/cm. The growth rate of the textured material was about 1 mm/h. A final oxygenation of the bar was performed at 450 °C during 72 h. A detailed description of the preparation process and a complete characterization of the microstructure, using optical and electronic microscopy, of Bridgman-grown samples similar to our B1 may be found in Ref. 28. The resulting directionally solidified material showed a quasi-single crystalline structure with a fine distribution of precipitates of the Y211 phase having a spheric-like shape. Our particular sample was observed with optical microscopy and analyzed with x-ray diffraction, which confirms its well-oriented single-domain nature. Other characteristics of sample B1, as well as for the other samples investigated in this work, are listed in Table I. Among these, of particular importance is the actual content of the Y211 phase, which was determined by measuring the paramagnetic susceptibility in the normal phase and fitting the results to a Curie-Weiss law in the high temperature range, according to the prescription given in Ref. 28. As shown in Table I, the final content of Y211 is substantially larger than the nominal composition of the presintered composite.

Samples TS-17, TS-25, and TS-30 were grown by the top-seeding method,[29] using melt-textured $NdBa_2Cu_3O_7$ seeds. The nominal contents of the Y211 phase added to the precursor composite are 17, 25, and 30 wt%, respectively. In all cases 1 wt% of CeO_2 was added to limit the coarsening of Y211 particles at high temperatures and to increase the liquid capillarity.[30] The addition of CeO_2 also changes the morphol-

TABLE I. Properties of the melt-textured YBCO samples investigated in this work. Listed are the method of preparation, the weight concentration of the Y211 phase determined from the normal state susceptibility, the in-plane transport critical current density at 5 K and the ratio between the perpendicular and in-plane resistivities at 300 K.

Sample	Method	%Y211	$j_c(10^5$ A/cm$^2)$	ρ_c/ρ_{ab}
B1	Bridgman	29		54.7
TS-17	Top-seeding	27	2.7	48.0
TS-25	Top-seeding	34		
TS-30	Top-seeding	44	2.8	5.8
TS-30-Ag	Top-seeding	40		

ogy of the Y211 particles, which acquire a more anisotropic needle-like shape.[31] Further details on the preparation and characterization of similar samples are given in Ref. 32. Our particular samples were x-rayed and studied for their electric properties. Some values obtained for the transport critical current parallel to the $Cu\text{-}O_2$ atomic planes at 5 K in a zero applied field are shown in Table I. Also shown is this table are the values for the ratio ρ_c/ρ_{ab} for the resistivities measured perpendicular and parallel to the $Cu\text{-}O_2$ planes at $T=300$ K. Both the resistivities are metallic-like. The increase in the nominal concentration of the Y211 phase leads to precipitates with a progressively reduced size[27] and to samples with enhanced pinning properties. The addition of the Y211 phase also reduces the density of microcracks in the samples, mainly those running parallel to the *ab* plane which separate the stacked platelets having a common *c*-axis, typical of the microstructure of the melt-textured cuprates.[27,28] However, as shown by the ratio ρ_c/ρ_{ab}, the progressive addition of Y211 tends to isotropize the composites.

The sample TS-30-Ag was prepared from a precursor nominally containing 30 wt% of Y211 and 15 wt% of Ag_2O. The top-seeding method was used. The addition of Ag to the melt-textured YBCO comes from an attempt to improve the superconducting and mechanical properties of these materials.[33] Studies of the morphology of the composites containing Ag_2O reveal that spherical-like Ag particles with a diameter between 10 and 50 μm are homogeneously distributed within the YBCO matrix.[33] The addition of Ag to the YBCO/Y211 composites eliminates the porosity usually observed in top-seeding samples and reduces the density of microcracks related to the platelet structure parallel to the *ab* plane. These morphological effects produce sizeable enhancements of the critical current density of composites containing Ag as compared to a reference sample having the same Y211 content, but no Ag_2O addition.[33]

B. Measurements

The measured samples were cut out from the melt-processed materials into the form of small and crystallographically oriented parallelepipeds. The cuts were performed with a diamond saw. Typical sample dimensions are $0.7\times0.9\times2.2$ mm, the largest being oriented parallel to the *c*-axis. Magnetization measurements were done with a Quantum Design MPMS-XL SQUID magnetometer, mostly operating in the RSO mode. The SQUID signal and the sample centering were visually monitored during the experimental runs. Magnetic fields from 1 Oe up to 50 kOe were applied either parallel or perpendicular to the *ab* plane. The misalignment of the field with respect to the sample edges was kept smaller than the 5° *c*-axis twist typical of the platelet structure in well oriented melt-textured YBCO.[28,29,31] Magnetic moments were measured as functions of the temperature according to the zero-field cooling (ZFC), field-cooled cooling (FCC), and field-cooled warming (FCW) prescriptions. The time-dependence of the FCC moment at fixed magnetic fields was studied. Experiments on the relaxation of the trapped FC magnetization after removing the applied field were also realized. All results were corrected for the corresponding demagnetization effects. These corrections were estimated by normalizing the ZFC diamagnetic susceptibility measured at low fields to the full shielding value. The values of the demagnetization factors so determined were further checked to estimations that approximate the samples' shape to an ellipsoid and make use of the calculations in Ref. 34. Differences between demagnetizing factors obtained from the two methods are within 10%.

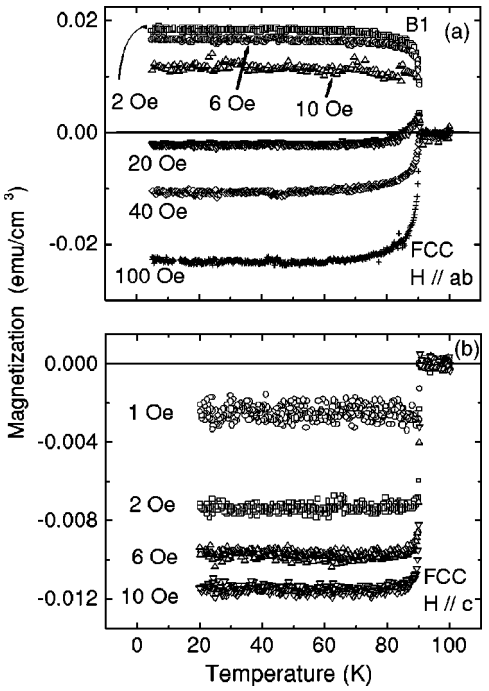

FIG. 1. (a) FCC magnetization for sample B1 in low fields applied parallel to the *ab* plane. The field magnitudes are indicated. (b) The same, for fields applied along the *c*-axis.

III. RESULTS

A. Low applied fields

Figure 1(a) shows the FCC magnetization as a function of the temperature for sample B1 in fields below 300 Oe applied parallel to the *ab* plane. Paramagnetic moments are observed in the whole temperature range below T_c when the

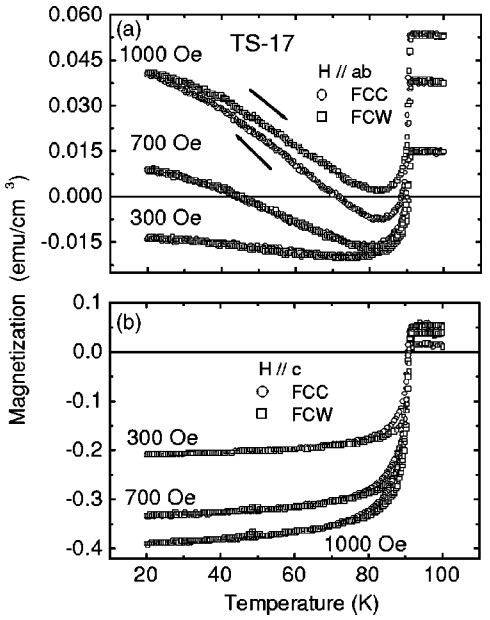

FIG. 2. (a) FCC and FCW magnetization for sample TS-17 in the quoted fields applied parallel to the *ab* plane. (b) The same, for $H \| c$.

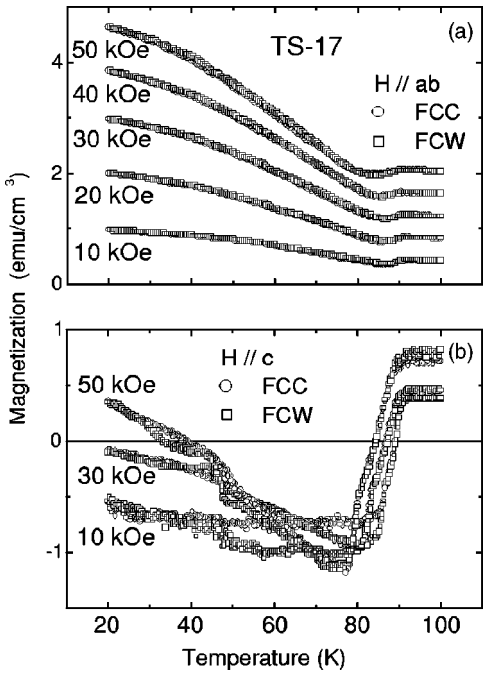

FIG. 3. FCC and FCW magnetizations for the TS-17 sample in the high-field range. (a) Results for $H \| ab$. (b) Results for $H \| c$. The field magnitudes are indicated.

applied field magnitude is smaller than 10 Oe. A small positive hump occurs in a short temperature range just below T_c in the magnetization measured at 20 Oe. Figure 1(a) presents the unique PME observed at low applied fields among all of our five samples. Even when fields of the same magnitude are applied along the *c*-axis of sample B1, no PME is observed. As one verifies in the results of Fig. 1(b), standard diamagnetic responses are obtained in this case. The signals presented in Fig. 1 are quite robust when faced with thermal cycling. The FCC and FCW magnetizations are coincident within the accuracy of the measurements and no change with time was detected in the FCC magnetization measured at $H = 2$ Oe and $T = 30$ K during $\Delta t \cong 4000$ s.

Results in Figs. 1 are qualitatively similar to those observed at low applied fields in polycrystalline Bi-based high-T_c superconductors[1–3] YBCO single crystals,[15,35] and Nb samples.[11,12,14] A difference is noticeable with respect to results in YBCO single crystals. In this case, the low-field PME was reported to occur when the field was applied along the *c*-axis, while in our melt-textured B1 sample the effect was detected only when *H* was parallel to the *ab* plane. Also worthy of note is the disappearance of the PME in our B1 sample upon polishing the sample's surface, as formerly observed in YBCO crystals[15] and Nb disks.[11]

B. Intermediate and high fields

Contrasting with the uniqueness of the PME observation at low fields, paramagnetic moments were detected at high enough fields in all of our samples. In some cases, as illustrated by the representative results in Fig. 2(a) for the TS-17 sample, weak paramagnetic signals are also detected in an intermediate field range roughly extending from 0.5 to 5 kOe. When appearing at such low field intensities, the paramagnetic moments have the characteristics of the high-field paramagnetic effect reported by Rykov *et al.*[23] in large crystals of YBCO or Terentiev *et al.*[13] in Nb thin films, but in general shows strong irreversibilities when the measurements are done with the FCC or FCW prescriptions. As seen in Fig. 2, in this field region, the contribution of the spin moment due to the Y211 particles may be comparable to that of the superconducting response, and becomes relevant to determine whether the sign of the total moment below T_c is positive or negative. We estimate the contribution of the Y211 particles to the total magnetization below T_c by extrapolating to low temperatures the linearly *T*-dependent behavior of the normal phase magnetization that is systematically observed in a certain temperature range just above T_c.

In the intermediate field range, the superconducting contribution to the magnetic moment in our melt-processed systems is strongly dependent on the cooling rate of the sample through T_c. As reported in Refs. 25 and 26, in few cases it is even possible to revert a diamagnetic signal into a paramagnetic one by simply cooling the sample at a high enough rate. Figure 2(b) also shows that the superconducting response may be strongly dependent on the field orientation, since only diamagnetic moments are seen when intermediate fields are applied along the *c*-axis in the TS-17 sample.

Figures 3 and 4 display HFPME observations for the TS-17 and TS-30 samples. These results show an important qualitative difference with respect to the low-field data: the magnitude of the paramagnetic moment increases monotonically with the applied field, even when the spin contribution from the Y211 particles is subtracted from the raw data. The temperature dependence of the HFPME in Figs. 3 and 4 is typical.[19] A diamagnetic dip is present below T_c; then the moment increases steadily as the temperature is lowered,

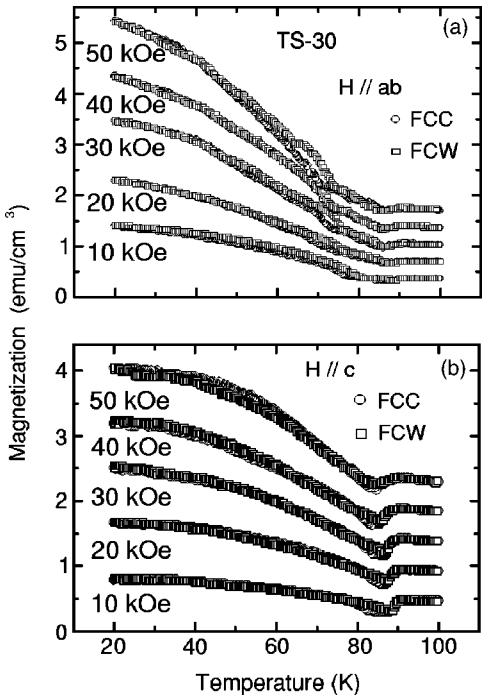

FIG. 4. The same as in Fig. 3, but for the TS-30 sample.

showing a tendency to saturate as T decreases towards zero. Weak FCC-FCW irreversibilities are observed and the HFPME is almost independent on the cooling rate in this field range. For the TS-17 sample, the magnetic moment is strongly anisotropic with respect to the field orientation. In Fig. 3(b), results for $H\|c$ are shown for this sample. In this case the total moment is much smaller than for $H\|ab$ and becomes truly paramagnetic only below 40 K at the highest applied field ($H=50$ kOe). For the TS-30 sample, the moment is also larger for $H\|ab$, but the anisotropy is much smaller in this case (see Fig. 4). The sample TS-25 behaves similarly to TS-17 and TS-30 in intermediate and high applied fields.

Figure 5 shows the field dependence of the FCW magnetization for the studied samples. In this figure the background moment due to the Y211 particles was removed. Figure 5(a) shows results for sample TS-17 at $T=30$ K. The anisotropy of the FC moment is smaller in TS-25 as compared to TS-17. This fact may be verified from the field dependence of the FCW magnetization shown in Fig. 5(b). Sample TS-30 is still less anisotropic, as shown by results in Fig. 5(c). The surfaces of this particular sample were polished until its shape acquired the form of an ellipsoid. Measurements of the FCC magnetization before and after shaping the sample TS-30 are shown in Fig. 6. The magnitude of the HFPME remains basically unaltered, although the temperature dependence of the FCC moment is slightly changed in the highest fields, and the diamagnetic dip below T_c becomes more pronounced.

The HFPME in samples B1 and TS-30-Ag present some noteworthy features that contrast with the regular tendencies displayed by results in the TS-17, -25, and -30 composites. The high-field effect in the Bridgman-grown B1 sample shows an anisotropy opposite to that observed in the top-

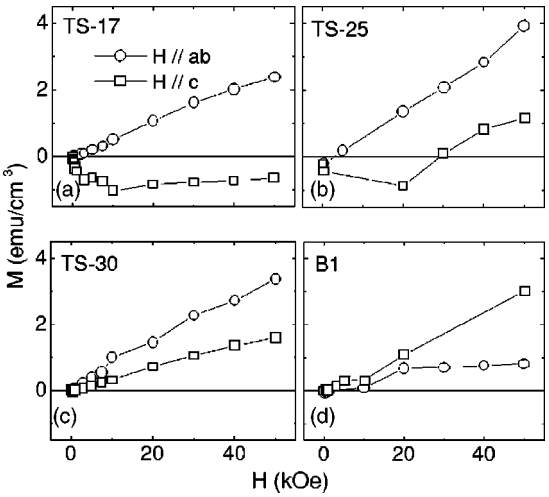

FIG. 5. FCW magnetization versus field at $T=30$ K for $H\|ab$ (circles) and $H\|c$ (squares), for samples (a) TS-17, (b) TS-25, (c) TS-30, and (d) B1. The magnetic contribution of the Y211 phase is subtracted.

seeding samples. In Fig. 5(d), one may verify that the field-dependence of the FCW magnetization at $T=30$ K is stronger when $H\|c$ for this sample. In Fig. 7, FCC and FCW magnetizations are shown as a function of the temperature for sample TS-30-Ag. In panel (a) data are obtained when the field is applied parallel to the ab plane. These results present the general trends of the HFPME shown by the other samples. In panel (b) of Fig. 7 are depicted the peculiar results obtained when the field is applied along the c-axis. Below the often observed negative dip near T_c, the FC moment displays a behavior reminding that of a spontaneous spin magnetization. The positive contribution to the moment rises abruptly at an almost field-independent temperature around 55 K, then shows a tendency to saturate at low temperatures at values varying roughly proportional to the applied field.

We point out that the total measured moment, including the spin contribution, is presented in Figs. 2, 3, and 4. In most cases the measured moment does not change sign and

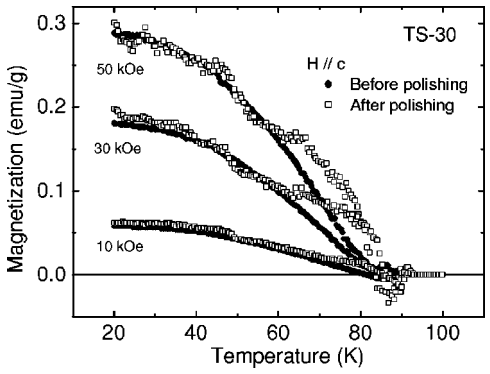

FIG. 6. FCC magnetization for the TS-30 sample measured in the indicated fields as a function of the temperature, before and after polishing its surfaces. Note that the magnetizations are quoted in emu/g to facilitate their quantitative comparison. The magnetic contribution of the Y211 particles is removed.

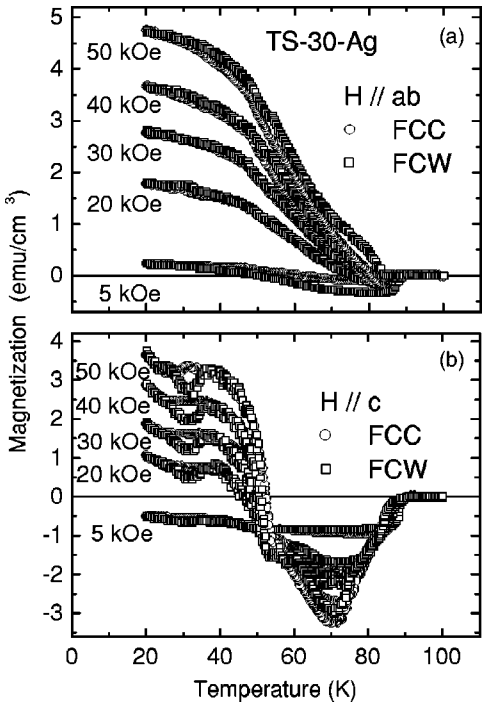

FIG. 7. FCC and FCW magnetizations for the sample TS-30-Ag measured in the indicated fields applied parallel to the (a) *ab* plane and (b) the *c*-axis.

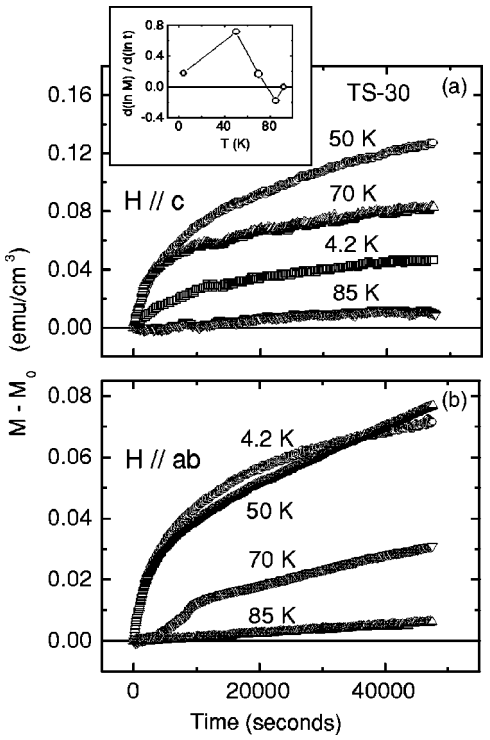

FIG. 8. Time dependence of the FCC magnetization for the sample TS-30 in the quoted temperatures. Measurements are performed at $H=2$ kOe applied parallel to (a) the *c*-axis, and (b) the *ab* plane. The inset in panel (a) shows the relaxation rate, $S=d(\ln M)/d(\ln t)$, as a function of T for the case $H\|c$.

remains positive for all temperatures. This fact reinforces our confidence that the HFPME observed below T_c is not due to a change-of-sign artifact produced by the MPMS software, as sometimes reported to occur in FCC measurements.[36] Concerning this issue, we also notice that our first observation of HFPME in melt-textured YBCO was made with a vibrating sample magnetometer.[25]

C. Time-dependence of the high-field paramagnetic effect

Figure 8 shows the time-dependence of the FCC magnetization for the sample TS-30, measured in $H=2$ kOe after cooling at 10 K/min from the normal phase to the quoted temperatures. Panels (a) and (b) of Fig. 8 show results obtained when the field is applied parallel or perpendicular to the *c*-axis, respectively. The inset in Fig. 8(a) shows the temperature dependence of the relaxation rate $S=d(\ln M)/d(\ln t)$ corresponding to the $H\|c$ data. The quantity S was obtained for time measurements exceeding 10^4 s, since strong deviations from the logarithmic time dependence for M are observed in shorter times. The magnetic field value chosen for experiments in Fig. 8 produces particularly large relaxation effects, and corresponds approximately to the penetration of the flux front until the center of the sample in ZFC experiments, so that in this field our sample is in a fully penetrated critical state. Relaxation experiments were also performed at $H=10$ kOe for this sample, with results similar to those shown in Fig. 8. Since the magnitude of the positive moments obtained in the FCC procedure are rather small when compared to that of a fully flux-excluded state, the variations of the magnetization in Fig. 8 are huge when compared to the first measured value, M_0. As an example, at $T=50$ K the FCC magnetization increases to about 100% of M_0 over 30 000 s. However, such an increase of M amounts to 0.1% of the ZFC magnetization measured at the same temperature and field.

Remarkable in the results of Fig. 8 is the fact that the paramagnetic moments obtained after field cooling the sample TS-30 relax monotonically to increasingly positive values. We have observed that this tendency remains unaltered for times exceeding 150 000 s.

The time-dependence of the FCC moment was also measured in the sample TS-17. In this case, the FCC moment in $H=2$ kOe is diamagnetic. However, the relaxation drives this moment to less negative values, indicating that extra flux is allowed to penetrate the sample in fixed temperatures. This behavior is just opposite to expectations based on a simple flux-creep scenario and contrasts to earlier observations in sintered[37] and single-crystal[38] samples of YBCO.

IV. DISCUSSION

A. PME at low fields

In spite of the large number of reports concerning the observation of PME in high- and low-T_c superconductors in small applied fields, this response occurs rarely. In fact, this effect appears only in a reduced number of samples under certain conditions. This is not different in our study. Among five melt-textured samples, the low-field PME was detected

only in the Bridgman grown B1 sample when fields smaller than 10 Oe were applied parallel to the *ab* plane. This fact makes it difficult to discuss our experiments within interpretations based on the polarization of orbital currents spontaneously generated by π Josephson junctions. Indeed, π junctions are expected to develop in planar structures oriented parallel to the *c*-axis, since the *d*-wave character of the superconducting wave function in the cuprates is primarily related to the $Cu\text{-}O_2$ atomic planes. The suppression of the PME upon polishing the sample surface is also difficult to conciliate with the π junction interpretation. This finding also suggests that the simple scenario of flux compression generated by inhomogeneous cooling of the sample[16] should be excluded. An additional indication in this sense comes from the observation that the low-field PME in sample B1 is independent of the cooling rate within the range $1-10$ K/min.

The dependence of the low-field PME in our melt-textured sample with the properties of its surface, as previously found by Lucht *et al.*[15] in YBCO single crystals and Thompson *et al.*[11] in Nb disks, does not favor either an interpretation as the one outlined by Nielsen *et al.*[22] which is based on characteristic features of the magnetic screening in multiply-connected superconductors. Their model was specifically based on the behavior of planar Josephson-junction arrays. The removal of the surface (in this case, the sample's perimeter) would leave the system invariant. Moreover, it is not clear that our bulk YBCO textured sample might be globally simulated as a Josephson medium for the particular situation where the field is applied parallel to the *ab* plane.

We suggest that the FC magnetic response of our B1 sample at low fields is dominated by the screening produced by Josephson currents flowing across certain surface defects. Specifically, we argue that extended planar defects, as the faults and microcracks separating the stacked platelets parallel to the *ab* plane in the case of our melt-textured samples, are essential to capture the whole magnetic flux under FC conditions. Such planar defects, acting as Josephson junctions, may trap Josephson vortices quite efficiently. Near the surface, the meandering of the peripherical screening current, that crosses the junctions at a depth corresponding to the Josephson penetration length (see a scheme in Fig. 9), may favor the entry of extra flux at the junction edges. A paramagnetic moment would then be generated. The low-field PME would then be a nearly equilibrium anti-Meissner effect, as first pointed out by Svedlindh *et al.*[1]

Our interpretation implies that the observation of the low-field PME is crucially dependent on the presence of a large density of extended planar defects oriented parallel to each other near the sample's surface. This is a stringent configuration that only occasionally occurs. Melt-processed and heavily twinned HTSC samples are favorable cases, as indeed verified experimentally.[2,3,35] The characteristic microstructure in small Bi-2212 grains showing PME as studied by electron microscopy[6] is also consistent with the above outlined picture. On the other hand, significant modifications of the PME are to be expected upon any mechanical treatment of the sample's surface that may remove or strongly alter the extended defects prone to trap Josephson vortices. It is indeed experimentally verified by many authors[11,12,15] that the removal of the surface layer by cutting, abrading or polishing have dramatic consequences on PME, even leading to its suppression. This is also the case for our B1 sample, which become diamagnetic upon gently polishing its surfaces.

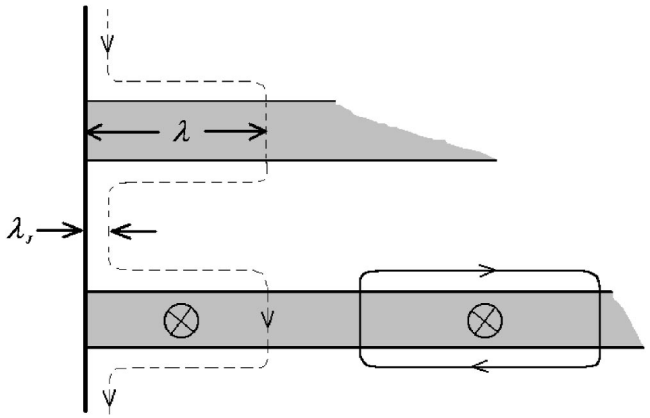

FIG. 9. Screening of the FC magnetization by Josephson currents (dashed line) that cross extended planar junctions oriented perpendicular to the sample surface at a depth corresponding to the Josephson penetration length, λ_J. Flux trapped in the junction's edge contributes to the low-field PME. A Josephson vortex is also represented in the scheme.

B. Paramagnetic effect at intermediate and high fields

Contrasting with the scarcity of the observations of paramagnetic moments at low fields, the occurrence of the paramagnetic effect at high applied fields is a general trend in our melt-textured samples. This only fact indicates that the effect at high fields has a different origin than its low-field counterpart. In addition, our results suggest that the strong pinning capacity is essential to the HFPME, since this is the distinctive characteristic of melt-processed YBCO samples. Pinning in these materials is strongly dependent on the interfaces between the superconducting phase and the Y211 phase. The most effective pinning centers are believed to be crystal defects associated with these interfaces, as stacking faults and dislocations in the YBCO matrix.[28,31]

In intermediate applied fields (0.5 kOe$<H<5$ kOe), the observed HFPME is caused by the inhomogeneous cooling of the sample below the superconducting transition, as shown by the extreme sensitivity of the effect on the cooling rate. Koshelev and Larkin[16] showed that in these conditions, flux near the edges of the sample may be expulsed towards its interior, leading to a compressed flux state which is stabilized by pinning when the superconductivity is fully established. Such a simple mechanism may not be dominant in higher applied fields range ($H>10$ kOe), where the HFPME systematically observed in our samples shows only a minor dependence on the cooling rate. However, the anisotropy of the HFPME results shown in Fig. 5 is evidence that pinning is also essential in this case. Microstructural studies of melt-processed YBCO shows that the addition of small amounts of CeO_2 to the starting mixture produces small and needle-like Y211 inclusions dispersed in the YBCO matrix.[31] As-

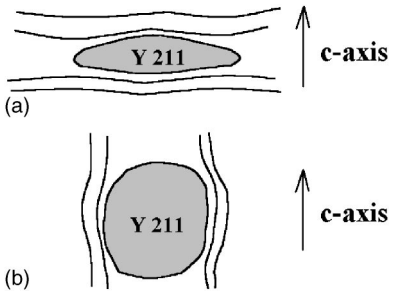

FIG. 10. Pinning by the Y211 particles (schematic). (a) Needle-like particles oriented parallel to the *ab* plane favor PME for $H \| ab$. (b) Spherical-like particles characteristic of the Bridgman grown sample, where PME is larger for $H \| c$.

suming that these particles are preferentially oriented parallel to the *ab* plane, the YBCO-Y211 interfacial area is enhanced along this orientation, reinforcing pinning for $H \| ab$ [see Fig. 10(a)]. As a possible consequence of this fact, the HFPME in the series of top-seeding samples is larger for the $H \| ab$ orientation. Figure 5 also shows that the HFPME anisotropy decreases as the weight fraction of the Y211 phase increases in the top-seeding samples. Indeed, as observed from results in Table I and Figs. 5(a)–5(c) the properties of melt-textured YBCO become more isotropic as the concentration of Y211 is augmented. Contrasting with the regular tendency shown by the TS series, in the B1 sample the high-field paramagnetic effect is larger for $H \| c$ [see Fig. 5(d)]. This result may also be understood on the basis of pinning by the YBCO-211 interfaces. In the Bridgman grown sample, CeO_2 was not added to the composite, and the Y211 particles are roughly spherical.[27,28] Thus, large interfacial areas between these inclusions and the YBCO matrix are expected to occur parallel to the *c*-axis, as shown schematically in Fig. 10(b). Consequently, pinning due to the YBCO-Y211 interfaces for the orientation $H \| c$ is enhanced as compared to the case of the top-seeding series, so that the HFPME anisotropy is inversed for the B1 sample.

We believe that the pinning capacity of the YBCO-Y211 interfacial regions exceeds largely that of other defects in bulk YBCO. Thus, flux compression at these regions in a FC experience may be so large that in some areas of the sample the vortex density is depleted below that expected from equilibrium. This opens a place for the admission of extra vortices into the sample, originating the paramagnetic response. Owing to the giant flux-creep typical of YBCO,[38] the YBCO-Y211 interfacial pinning acts as a pump of vortices, increasing the nearby flux density as time evolves and producing the anomalous relaxation of the FC magnetic moment towards more positive values.

Although the strong deviations from a simply time-logarithmic relaxation, results in Fig. 8 show that the relaxation rate goes through a maximum at temperatures well below T_c, as earlier found in flux creep processes in single-crystal YBCO.[38] Thus, our anomalous relaxation results, as well as those reported by Terentiev *et al.*[13] in Nb thin films, seem to indicate that the formation of a flux compressed state modulated by pinning and strong flux creep processes is indeed at the origin of the HFPME.

The HFPME in the TS-30-Ag composite, shown in Fig. 7, reproduces in part the behavior observed in the other samples. When the field is applied parallel to the *ab* plane, the effect is qualitatively the same. For instance, the field dependence of the paramagnetic moment anisotropy at $T = 30$ K is quite similar to that shown by the sample TS-30 [see Fig. 5(d)], which has the same amount of the Y211 phase. This indicates that at low temperatures the pinning mechanism for both samples is the same. On the other hand, when $H \| c$ the temperature dependence of the HFPME resembles that of a spin magnetization which is suppressed at $T_s \cong 55$ K, independently of the applied field magnitude [see Fig. 7(b)]. It is however difficult to associate the HFPME behavior below T_s to an anisotropic spin magnetization, since one can hardly conceive that the mere addition of Ag particles to the melt-processed YBCO-Y211 composite would favor the appearance of ferromagnetic precipitates, or of some field-induced weakly ferromagnetic response in the sample. Alternatively, one might suppose that some pinning mechanism, which is effective for $H \| c$, abruptly ceases to act above T_s. Thus, the liberated fraction of the flux may be expelled from the sample, suppressing the HFPME above this characteristic temperature. If correct, this interpretation suggests that the phenomenon depicted in Fig. 7(b) may be taken as an evidence of the postulated depinning transition,[39] which considers that the depinning of the flux lattice from the material's defect structure may proceed as a phase transition.

V. CONCLUSIONS

We have presented experimental results on the field-cooled magnetization of five different melt-textured YBCO samples containing large amounts of the Y211 phase. Our experiments were performed in a broad range of applied fields, ranging from 1 Oe up to 50 kOe. In the low-field limit, we have observed a paramagnetic Meissner moment only in a sample grown with the Bridgman method for the configuration $H \| ab$ ($H < 20$ Oe). This low-field PME is a quasi-equilibrium effect similar to those observed in Bi-2212 polycrystals,[1–3] YBCO single-crystals,[15,35] Nb disks,[11,12] and other systems. We outline an interpretation attributing this low-field PME to the meandering of Josephson screening currents that flow across extended planar defects occasionally occurring at the sample's surface.

Contrasting with the unique observation of PME at low magnetic fields, paramagnetic moments below T_c were observed in all of the samples studied by us in strong enough fields. This high-field paramagnetic effect[19] occurs both for $H \| ab$ and $H \| c$, increases monotonically with the applied field within the studied range, and shows significant time-dependence. Interestingly enough, the relaxation is such that the paramagnetic moment increases as a function of time. The anisotropy of the HFPME regarding the orientation of the magnetic field with respect to the crystallographic axes is dependent on the sample microstructure. For samples grown with the top-seeding method, this anisotropy is such that the paramagnetic moment is larger for the orientation $H \| ab$, whereas for the Bridgman-grown sample the effect is more

pronounced for $H \| c$. This property suggests that the pinning by the Y211 particles dispersed in the YBCO melt-processed matrix is relevant to the occurrence of the HFPME in our samples, since the geometric form and orientation of these inclusions are crucially dependent on the method of preparation. We propose that the formation of a flux-compressed state modulated by pinning and strong flux-creep is at the origin of the HFPME in our samples. However, a detailed theoretical description of this effect is still lacking since the existing flux-compressed scenarios[16,17] do not take into consideration the crucial role of the pinning mechanism, nor the importance of vortex dynamics. One should also notice that the Y211 inclusions are magnetic. The problem of interaction of vortices with magnetic particles is largely unexplored,[40] so that nontrivial effects as the flux compression resulting in the HFPME and the anomalous relaxation of the FC moment towards positive values might not be dissociated from this scenario.

[1] P. Svedlindh, K. Niskanen, P. Norling, P. Nordblad, L. Lundgren, B. Lönnberg, and T. Lundström, Physica C **162–164**, 1365 (1989).

[2] W. Braunish, N. Knauf, V. Kataev, S. Neuhausen, A. Grütz, A. Kock, B. Roden, D. Khomskii, and D. Wohlleben, Phys. Rev. Lett. **68**, 1908 (1992).

[3] W. Braunish, N. Knauf, G. Bauer, A. Kock, A. Becker, B. Freitag, A. Grütz, V. Kataev, S. Neuhausen, B. Roden, D. Khomskii, D. Wohlleben, J. Bock, and E. Preisler, Phys. Rev. B **48**, 4030 (1993).

[4] F. V. Kusmartsev, Phys. Rev. Lett. **69**, 2268 (1992).

[5] M. Sigrist and T. M. Rice, Rev. Mod. Phys. **67**, 503 (1995).

[6] B. Freitag, B. Büchner, N. Knauf, B. Roden, H. Micklitz, A. Freimuth, and V. Kataev, Europhys. Lett. **45**, 393 (1999).

[7] J. Magnusson, J. O. Anderson, M. Björnander, P. Nordblad, and P. Svedlindh, Phys. Rev. B **51**, 12776 (1995).

[8] J. R. Kirtley, A. C. Mota, M. Sigrist, and T. M. Rice, J. Phys.: Condens. Matter **10**, L97 (1998).

[9] J. Magnusson, E. Papadopoulou, P. Svedlindh, and P. Nordblad, Physica C **297**, 317 (1998).

[10] E. L. Papadopoulou, P. Nordblad, P. Svedlindh, R. Schöneberger, and R. Gross, Phys. Rev. Lett. **82**, 173 (1999).

[11] D. J. Thompson, M. S. M. Minhaj, L. E. Wenger, and J. T. Chen, Phys. Rev. Lett. **75**, 529 (1995).

[12] P. Kostic, B. Veal, A. P. Paulikas, U. Welp, V. R. Todt, C. Gu, U. Geiser, J. M. Williams, K. D. Carlson, and R. A. Klemm, Phys. Rev. B **53**, 791 (1996).

[13] A. Terentiev, D. B. Watkins, L. E. De Long, D. J. Morgan, and J. B. Ketterson, Phys. Rev. B **60**, R761 (1999).

[14] W. A. Wortiz, P. N. Lisboa-Filho, W. A. C. Passos, and F. M. Araújo-Moreira, Physica C **361**, 267 (2001).

[15] R. Lucht, H. V. Löhneysen, H. Claus, M. Kläser, and G. Müller-Vogt, Phys. Rev. B **52**, 9724 (1995).

[16] A. E. Koshelev and A. I. Larkin, Phys. Rev. B **52**, 13559 (1995).

[17] V. V. Moshchalkov, X. G. Qiu, and V. Bruyndoncx, Phys. Rev. B **55**, 11793 (1997).

[18] Yu V. Obukhov, J. Supercond. **11**, 733 (1998).

[19] A. K. Geim, S. V. Dubonos, J. G. S. Lok, M. Henini, and J. C. Maan, Nature (London) **396**, 144 (1998).

[20] F. M. Araújo-Moreira, P. Barbara, A. B. Cawthorne, and C. J. Lobb, Phys. Rev. Lett. **78**, 4625 (1997); P. Barbara, F. M. Araújo-Moreira, A. B. Cawthorne, and C. J. Lobb, Phys. Rev. B **60**, 7489 (1999).

[21] A. P. Nielsen, A. B. Cawthorne, P. Barbara, F. C. Wellstood, C. J. Lobb, R. S. Newrock, and M. G. Forrester, Phys. Rev. B **62**, 14380 (2000).

[22] C. De Leo, G. Rotoli, P. Barbara, A. P. Nielsen, and C. J. Lobb, Phys. Rev. B **64**, 144518 (2001).

[23] A. I. Rykov, S. Tajima, and F. V. Kusmartsev, Phys. Rev. B **55**, 8557 (1997).

[24] M. S. Li, Phys. Rep. **376**, 133 (2003).

[25] F. T. Dias, P. Pureur, P. Rodrigues, Jr., and X. Obradors, Physica C **341–348**, 1377 (2000).

[26] F. T. Dias, P. Pureur, P. Rodrigues, Jr., and X. Obradors, Physica C **354**, 219 (2001).

[27] S. Piñol, V. Gomis, B. Martinez, A. Labarte, J. Fontcuberta, and X. Obradors, J. Alloys Compd. **195**, 11 (1993).

[28] F. Sandiumenge, S. Piñol, X. Obradors, E. Snoeck, and C. Roucau, Phys. Rev. B **50**, 7032 (1994).

[29] K. Salama and D. F. Lee, Supercond. Sci. Technol. **12**, R27 (1999).

[30] S. Piñol, F. Sandiumenge, B. Martínez, V. Gomis, J. Fontcuberta, X. Obradors, E. Snoeck, and C. Roucau, Appl. Phys. Lett. **65**, 1448 (1994).

[31] C.-J. Kim and G.-W. Hong, Supercond. Sci. Technol. **12**, R27 (1999).

[32] X. Obradors, R. Yu, F. Sandiumenge, B. Martínez, N. Vilalta, V. Gomis, T. Puig, and S. Piñol, Supercond. Sci. Technol. **10**, 884 (1997).

[33] E. Mendoza, T. Puig, E. Varesi, A. E. Carrillo, J. Plaim, and X. Obradors, Physica C **334**, 7 (2000).

[34] J. A. Osborn, Phys. Rev. **67**, 351 (1945).

[35] S. Riedling, G. Bräuchle, R. Lucht, K. Röhberg, H. V. Löhneysen, H. Claus, A. Erb, and G. Müller-Vogt, Phys. Rev. B **49**, 13283 (1994).

[36] F. J. Blunt, A. R. Perry, A. M. Campbell, and R. S. Liu, Physica C **175**, 539 (1991).

[37] P. Norling, P. Svedlindh, P. Nordblad, L. Lundgren, and P. Przyslupsky, Physica C **153–155**, 314 (1988).

[38] Y. Yeshurun and A. P. Malozemoff, Phys. Rev. Lett. **60**, 2202 (1988).

[39] Y. Kopelevich and P. Esquinazi, Solid State Commun. **114**, 241 (2000).

[40] D. J. Morgan and J. B. Ketterson, Phys. Rev. Lett. **80**, 3614 (1998).